Article

Delayed fluorescence from inverted singlet and triplet excited states

https://doi.org/10.1038/s41586-022-05132-y

Received: 29 April 2021

Accepted: 21 July 2022

Published online: 14 September 2022

Open access

Check for updates

Naoya Aizawa[1,2,3]✉, Yong-Jin Pu[1,4]✉, Yu Harabuchi[5,6], Atsuko Nihonyanagi[1], Ryotaro Ibuka[1], Hiroyuki Inuzuka[1], Barun Dhara[1], Yuki Koyama[1,4], Ken-ichi Nakayama[2], Satoshi Maeda[5,6], Fumito Araoka[1] & Daigo Miyajima[1]✉

Hund's multiplicity rule states that a higher spin state has a lower energy for a given electronic configuration[1]. Rephrasing this rule for molecular excited states predicts a positive energy gap between spin-singlet and spin-triplet excited states, as has been consistent with numerous experimental observations over almost a century. Here we report a fluorescent molecule that disobeys Hund's rule and has a negative singlet–triplet energy gap of −11 ± 2 meV. The energy inversion of the singlet and triplet excited states results in delayed fluorescence with short time constants of 0.2 μs, which anomalously decrease with decreasing temperature owing to the emissive singlet character of the lowest-energy excited state. Organic light-emitting diodes (OLEDs) using this molecule exhibited a fast transient electroluminescence decay with a peak external quantum efficiency of 17%, demonstrating its potential implications for optoelectronic devices, including displays, lighting and lasers.

The spin multiplicity of molecular excited states plays a crucial role in organic optoelectronic devices. In the case of OLEDs, recombination of charge carriers leads to the formation of singlet and triplet excited states in a 1:3 ratio. This spin statistics limits the internal quantum efficiency of OLEDs and leads to the energy loss owing to the spin-forbidden nature of triplet excited states to emit photons. To overcome this issue, two strategies for harvesting the 'dark' triplet excited states as photons have been established. The first relies on organometallic complexes with transition metals, such as iridium and platinum, which induce a large spin–orbit coupling to allow triplet states to emit photons as phosphorescence[2–4]. The other uses organic molecules that exhibit thermally activated delayed fluorescence (TADF)[5–7]. This class of materials has energetically close singlet and triplet excited states, in which ambient thermal energy upconverts the triplet states into the singlet states through reverse intersystem crossing (RISC). Although the concept of TADF has the advantage of eliminating the need for transition metals, the resultant temporally delayed fluorescence typically has a time constant in the microsecond or even millisecond range, which is long enough for detrimental bimolecular annihilations, such as triplet–triplet annihilation and triplet–polaron annihilation, to compete with delayed fluorescence. These bimolecular annihilations lead to the decrease in device efficiency under high current densities, known as efficiency roll-off in OLEDs[8,9], and also generate high-energy excitons that are suspected to cause chemical degradation of materials, particularly in blue OLEDs[10]. The research community has thus focused on minimizing the singlet–triplet energy gap (ΔE_{ST}) to accelerate the upconversion by thermal activation[7]. Alternatively, an ideal case would be thermodynamically favourable downconversion with negative ΔE_{ST}, which is not expected if applying Hund's multiplicity rule to the lowest-energy excited state. Herein, we demonstrate experimental evidence of the existence of highly fluorescent organic molecules that disobey Hund's rule and possess negative ΔE_{ST} for constructing efficient OLEDs.

Numerous observations of positive ΔE_{ST} in molecular excited states are generally understood by the exchange interaction, the quantum-mechanical effect involving Pauli repulsion, which stabilizes triplet states relative to singlet states[11]. ΔE_{ST} is simply equal to twice the positive exchange energy if the lowest-energy singlet and triplet excited states (S_1 and T_1) have the same single-excitation configuration[11]. Although there is general agreement that ΔE_{ST} must be positive, potentially negative ΔE_{ST} has been discussed in nitrogen-substituted phenalene analogues, such as cycl[3.3.3]azine and heptazine, during the past two decades[12–21]. Recent theoretical studies have also suggested the possibility of negative ΔE_{ST} in these molecules by accounting for double-excitation configurations in which two electrons of occupied orbitals have been promoted out to virtual orbitals[15–19] (Supplementary Fig. 1). Because the Pauli exclusion principle restricts the accessible double-excitation configurations in T_1, an effective admixture of such configurations stabilizes S_1 relative to T_1. If this stabilization overcomes the exchange energy, ΔE_{ST} could be a negative value (Fig. 1a). However, to the best of our knowledge, none of the molecules has been experimentally identified with negative ΔE_{ST} and the resultant delayed fluorescence from inverted singlet and triplet excited states (DFIST). We note that the accounting for double-excitation configurations has proved crucial to theoretically reproduce the small but positive ΔE_{ST} of 5,9-diphenyl-5,9-diaza-13b-boranaphtho[3,2,1-*de*]anthracene (DABNA-1) (0.15 eV)[22,23].

Pioneering computational calculations[15] inspired us to focus on heptazine as a potential class of molecules that exhibit DFIST. Correlated wave function theories suggested that S_1 of heptazine lies 0.2–0.3 eV

[1]RIKEN Center for Emergent Matter Science (CEMS), Wako, Japan. [2]Department of Applied Chemistry, Graduate School of Engineering, Osaka University, Suita, Japan. [3]Precursory Research for Embryonic Science and Technology (PRESTO), Japan Science and Technology Agency (JST), Kawaguchi, Japan. [4]Graduate School of Organic Materials Science, Yamagata University, Yonezawa, Japan. [5]Department of Chemistry, Faculty of Science, Hokkaido University, Sapporo, Japan. [6]Institute for Chemical Reaction Design and Discovery (WPI-ICReDD), Hokkaido University, Sapporo, Japan. ✉e-mail: aizawa@chem.eng.osaka-u.ac.jp; yongjin.pu@riken.jp; daigo.miyajima@riken.jp

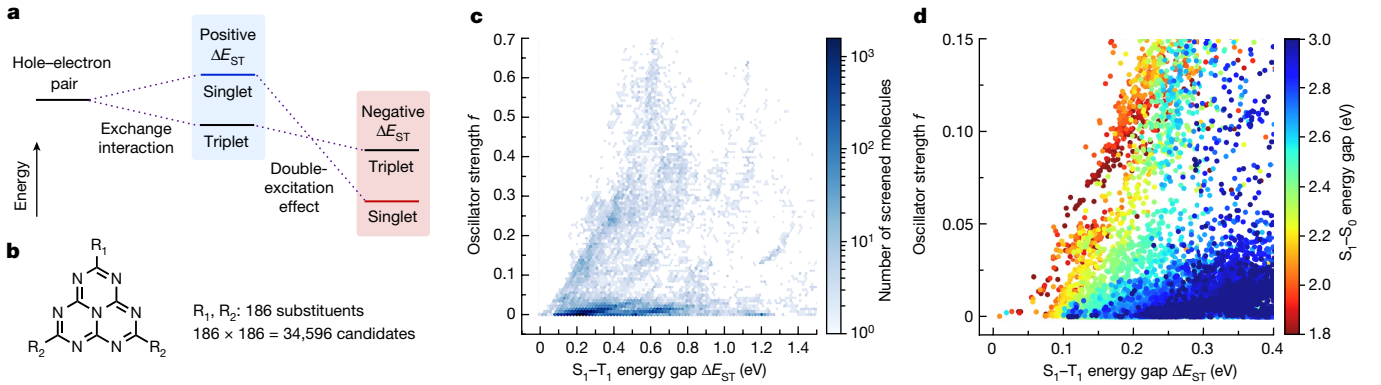

Fig. 1 | Computational screening of heptazine analogues. a, Schematic diagram of singlet and triplet excited states split in energy by the exchange interaction (middle) and then inverted by including the double-excitation effect (right). **b**, Molecular structures of the heptazine analogues examined in the computational screening. **c**, Number of screened molecules as a function of ΔE_{ST} and f calculated by TDDFT. **d**, S_1–S_0 energy gaps as a function of ΔE_{ST} and f calculated by TDDFT.

below T_1, although S_1 is a 'dark' state, meaning that the electronic transition to the ground state (S_0) is dipole-forbidden and the oscillator strength (f) is zero in the D_{3h} symmetry point group. Notably, the heptazine core is shared by several synthesized molecules that exhibit intense TADF[24,25] with positive ΔE_{ST} (refs. [26,27]). Furthermore, the recent computational screening by Pollice et al. has demonstrated that appropriate chemical modifications of heptazine recover f while retaining negative ΔE_{ST} (ref. [19]). As such, we introduced 186 different substituents to heptazine to generate 34,596 candidate molecules for computational screening. The structures of all substituents are available in Supplementary Fig. 2. To ensure the synthetic feasibility, at most two distinct types of substituents were introduced to the heptazine core as R_1 and R_2 (Fig. 1b). We used standard linear-response time-dependent density functional theory (TDDFT) to calculate ΔE_{ST} and f, which are more affordable in computational cost than those calculated by correlated wave function theories. Although the commonly used adiabatic approximation in TDDFT does not account for double-excitation character[16,28], the properties calculated by TDDFT are still useful to prescreening for narrowing the list of the candidate molecules before the high-cost calculations and experimental evaluation, as both S_1 and T_1 of heptazine are almost dominated by the single-excitation configuration between the highest occupied molecular orbital (HOMO) and the lowest unoccupied molecular orbital (LUMO)[15].

Figure 1c shows the statistics of the screened molecules as a function of ΔE_{ST} and f calculated by TDDFT. A well-known trade-off between small ΔE_{ST} and large f is evident from this particular dataset of heptazine analogues. Although balancing such a trade-off is a key concern in recent synthetic efforts on TADF materials, Fig. 1c demonstrates the optimal combinations of ΔE_{ST} and f for which one parameter can no longer be improved without sacrificing the other. Figure 1d further visualizes the trade-off between ΔE_{ST} and f for each fluorescence colour. The screening data suggest 5,264 promising candidates to show fluorescence across the entire visible spectrum, with $\Delta E_{ST} < 0.35$ eV and $f > 0.01$. Setting the range of the vertical S_1–S_0 energy gap to 2.70–2.85 eV for blue fluorescence further narrows down the candidates to 1,028 molecules, corresponding to 2.97% of all the screened molecules. We then assessed their synthetic feasibility and selected two heptazine analogues $HzTFEX_2$ and $HzPipX_2$ (Fig. 2a) for further evaluation. We note that these molecules recover f while retaining small ΔE_{ST} ($f = 0.010$ and 0.015 and $\Delta E_{ST} = 210$ and 334 meV for $HzTFEX_2$ and $HzPipX_2$, respectively). This trend is consistent with the recent computational screening on heptazine analogues with asymmetrical substitutions[19].

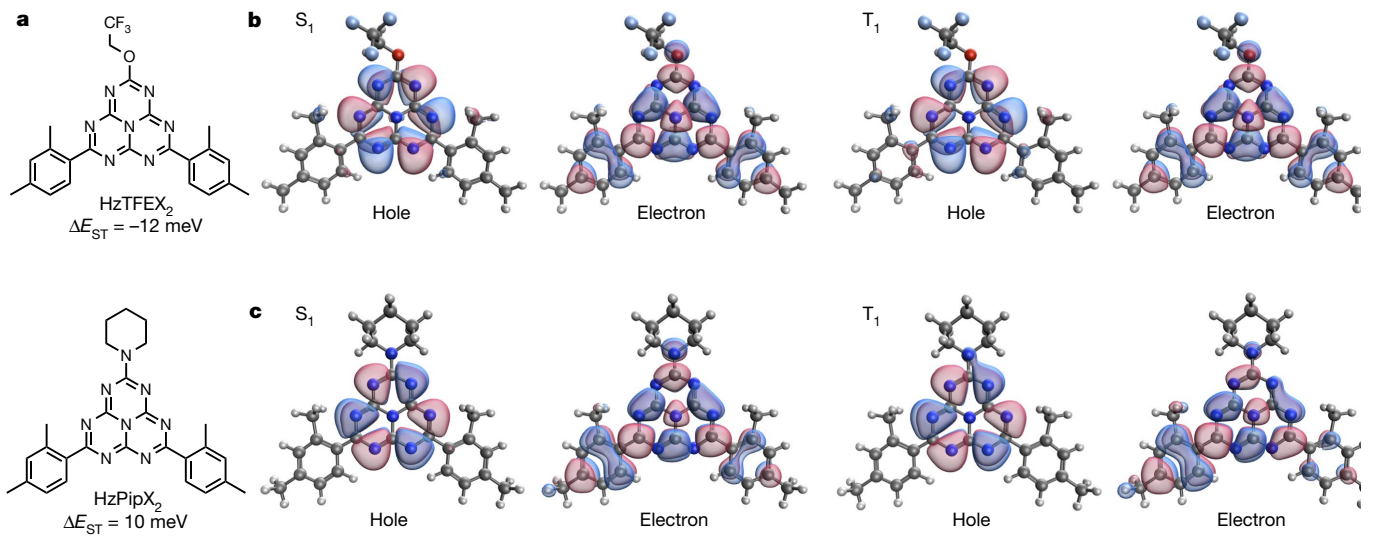

Fig. 2 | Lead candidate molecules $HzTFEX_2$ and $HzPipX_2$. a, Molecular structures of $HzTFEX_2$ and $HzPipX_2$ with ΔE_{ST} calculated by EOM-CCSD. **b**,**c**, Dominant pair of NTOs of S_1 and T_1 of $HzTFEX_2$ (**b**) and $HzPipX_2$ (**c**) for the EOM-CCSD calculations.

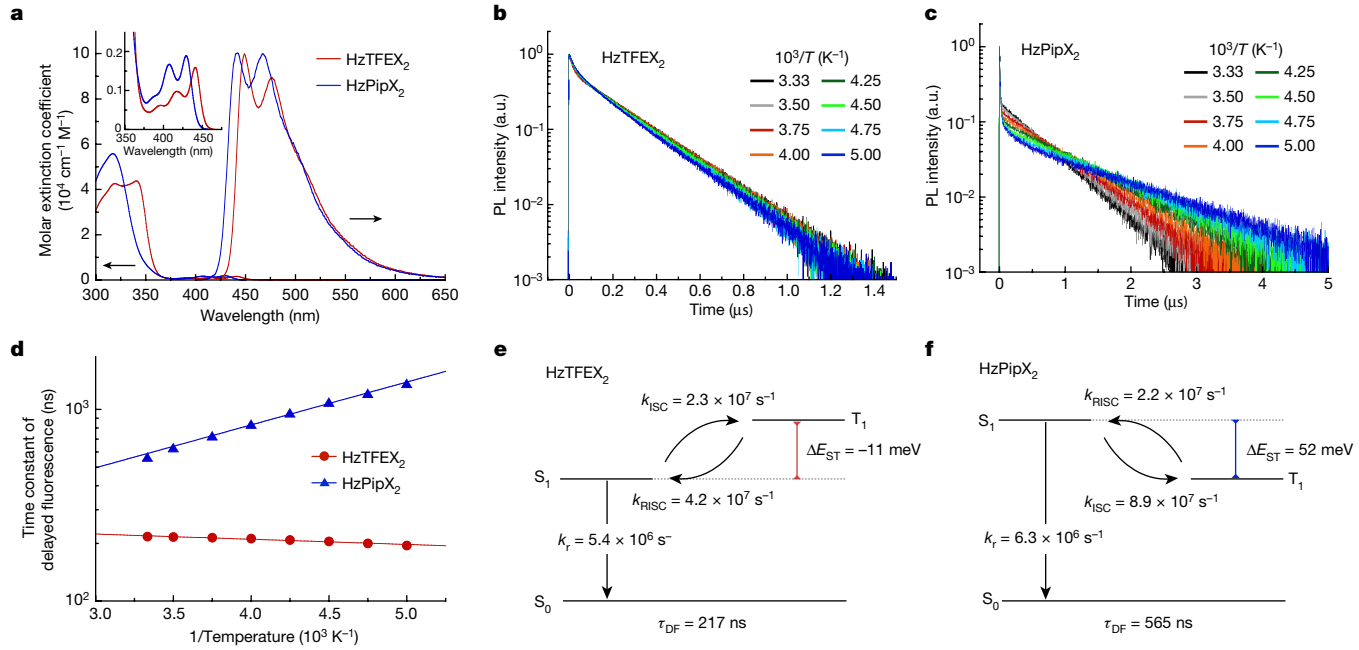

Fig. 3 | Photophysical properties of HzTFEX$_2$ and HzPipX$_2$ in deaerated toluene solutions. a, Steady-state absorption and PL spectra of HzTFEX$_2$ and HzPipX$_2$. The inset is the magnified view of the absorption spectra. **b**,**c**, Transient PL decays of HzTFEX$_2$ (**b**) and HzPipX$_2$ (**c**) at varying temperatures. **d**, Temperature dependence of τ_{DF} of HzTFEX$_2$ and HzPipX$_2$; the solid lines in **d** represent the fits of τ_{DF} to a single exponential in inverse temperature. **e**,**f**, Schematic diagram of the excited states and the associated transitions of HzTFEX$_2$ (**e**) and HzPipX$_2$ (**f**).

To examine whether HzTFEX$_2$ and HzPipX$_2$ could have negative ΔE_{ST}, we computed their S_1 and T_1 by correlated wave function theories. Equation-of-motion coupled cluster with single and double excitation (EOM-CCSD)[29] calculations predict HzTFEX$_2$ to possess negative ΔE_{ST} of −12 meV, affirming its potential for exhibiting DFIST. In comparison, ΔE_{ST} calculated for HzPipX$_2$ remains at a positive value of 10 meV, which is comparable with those of the current state-of-the-art TADF materials[30–38]. Figure 2b,c shows the dominant pair of natural transition orbitals (NTOs)[39] for S_1 and T_1. In both molecules, the hole orbitals are exclusively localized on the peripherical six nitrogen atoms of the heptazine core, whereas the electron orbitals are localized on the central nitrogen atom and the carbon atoms of the core, as well as on the substituents. The spatial separation of these orbitals indicates that the exchange interaction is weak, resulting in nearly degenerate S_1 and T_1 in the single-excitation picture. Similar spatial separations of NTOs have also been found in the multi-resonant TADF materials, such as DABNA-1 (refs. [22,23]). In this situation, the stabilization of S_1 by including the double-excitation configurations becomes more dominant to determine the sign of ΔE_{ST}. Indeed, S_1 of both molecules comprise double-excitation configurations with weights of around 1% described as the sum of the squares of the doubles amplitudes in EOM-CCSD, which are slightly higher than those of T_1. Two other wave-function-based calculations using second-order algebraic diagrammatic construction (ADC(2))[40] and complete active space with second-order perturbation theory (CASPT2)[41] further validate the inversion of S_1 and T_1 in HzTFEX$_2$ with calculated ΔE_{ST} of −34 meV and −184 meV, respectively. However, for HzPipX$_2$, the two methods also invert ΔE_{ST} (−12 meV with ADC(2) and −171 meV with CASPT2) as compared with the positive value of 10 meV predicted with EOM-CCSD (Supplementary Table 1). This variation in estimates of ΔE_{ST} highlights the current limitations of excited-state calculations and demands conclusive experimental evaluation. We note that ΔE_{ST} calculated by other second-order methods are given in the Supplementary Information, as well as the dependence of the choice of the guess orbitals and the size of the active space on the CASPT2 results.

HzTFEX$_2$ and HzPipX$_2$ were synthesized by nucleophilic aromatic substitution of 2,5,8-trichloroheptazine with corresponding alcohol or amine, followed by Friedel–Crafts reactions with *m*-xylene. The details of the synthesis and characterization are given in the Supplementary Information. The photophysical properties of the two molecules were evaluated in deaerated toluene solutions (Fig. 3a and Extended Data Table 1). The steady-state absorption spectra of HzTFEX$_2$ and HzPipX$_2$ comprise the lowest-energy absorption band centred at 441 nm and 429 nm, respectively, with small molar absorption coefficients on the order of 10^3 M^{-1} cm^{-1}, reflecting the spatial separation between the hole and electron NTOs computed for S_1 of each molecule. On photoexcitation, HzTFEX$_2$ exhibits blue emission with a peak wavelength (λ_{PL}) of 449 nm and a photoluminescence (PL) quantum yield (Φ_{PL}) of 74%, whereas slightly blue-shifted λ_{PL} of 442 nm and similar Φ_{PL} of 67% are observed for HzPipX$_2$. These energy differences in absorption and emission are also predicted by TDDFT calculations and are attributed to the stronger electron-donating effect of the piperidyl group in HzPipX$_2$ than that of 2,2,2-trifluoroethoxy group in HzTFEX$_2$. In aerated toluene solutions, Φ_{PL} of HzTFEX$_2$ and HzPipX$_2$ decrease to 54% and 37%, respectively. Because atmospheric O_2 can quench molecular triplet excited states and the change in Φ_{PL} is reversible, we ascribe the blue emissions of the two molecules, at least partially, to delayed fluorescence through forward intersystem crossing (ISC) and RISC between S_1 and T_1. This assumption is supported by transient absorption decay measurements on HzTFEX$_2$, which scrutinized ISC from S_1 to T_1 as the signal decay of S_1 at 700 nm and the signal growth of T_1 at 1,600 nm, followed by the persistent signal decays of both S_1 and T_1 (Extended Data Fig. 1). We also note that both decays have similar time constants (223 ns for S_1 and 210 ns for T_1), indicating the steady-state condition with the constant population ratio maintained by ISC and RISC.

To show the excited-state kinetics of the two molecules in detail, we performed transient PL decay measurements at varying temperatures (Fig. 3b,c and Supplementary Fig. 3 for the log–log representation). Both molecules exhibit biexponential transient PL decays, which comprise nanosecond-order prompt fluorescence followed by sub-microsecond delayed fluorescence with temperature-dependent time constants.

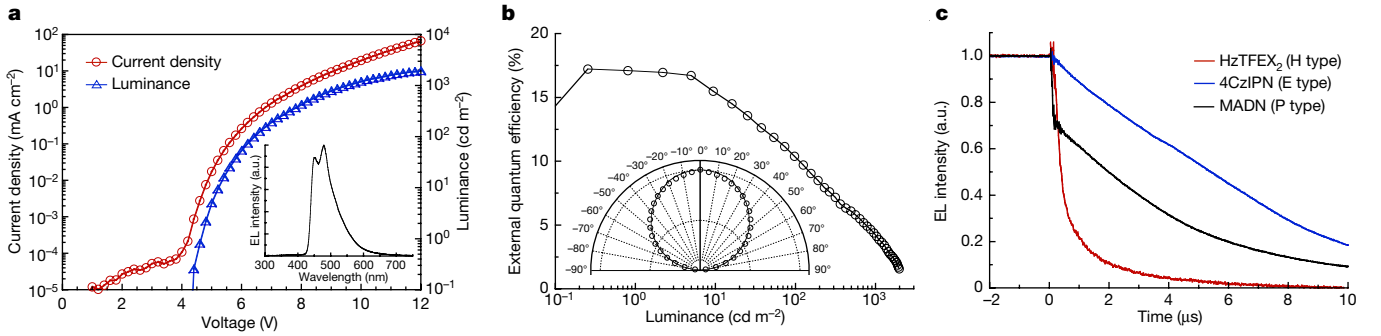

Fig. 4 | OLED performance. a,**b**, Current density–voltage–luminance characteristics (**a**) and external quantum efficiency–luminance characteristics (**b**) of the fabricated OLED using $HzTFEX_2$; the inset in **a** shows the EL spectra measured at 1.0 mA and the inset in **b** represents the viewing-angle dependence of the luminance, which is almost consistent with the Lambertian distribution. **c**, Transient EL decays of the OLEDs using $HzTFEX_2$, 4CzIPN and MADN, respectively, measured in pulse operation with square-wave voltages of 8 V and −4 V.

Remarkably, the time constant of delayed fluorescence (τ_{DF}) of $HzTFEX_2$ gradually decreases from 217 ns to 195 ns with decreasing temperature from 300 K to 200 K (Fig. 3d). This anomalous temperature dependence of τ_{DF} indicates that S_1 lies energetically below T_1, for which lowering the temperature shifts the steady-state population towards emissive S_1 relative to dark T_1 and thus accelerates the delayed fluorescence (that is, decreases τ_{DF}). In comparison, τ_{DF} of $HzPipX_2$ increases from 565 ns to 1,372 ns by the same temperature decrease, as has been similarly observed in conventional TADF materials[5–7]. It is worth noting that τ_{DF} of $HzTFEX_2$ is much shorter than emission time constants ever reported for TADF materials[30–38] and phosphorescent materials[2–4] used for efficient OLEDs, which are typically in the microsecond range.

We further analysed the temperature-dependent PL decay kinetics with the underlying rate equation. In the absence of phosphorescence and non-radiative decay of T_1 to S_0, the rate equation for the populations of S_1 and T_1 is given by

$$\frac{\mathrm{d}}{\mathrm{d}t}\begin{pmatrix} S_1 \\ T_1 \end{pmatrix} = \begin{pmatrix} -(k_r + k_{nr} + k_{ISC}) & k_{RISC} \\ k_{ISC} & -k_{RISC} \end{pmatrix}\begin{pmatrix} S_1 \\ T_1 \end{pmatrix} \quad (1)$$

in which k_r, k_{nr}, k_{ISC} and k_{RISC} are the rate constants of radiative decay of S_1 to S_0, non-radiative decay of S_1 to S_0, ISC of S_1 to T_1 and RISC of T_1 to S_1, respectively. By numerically fitting equation (1) to the PL decay data at 300 K, we found that RISC is faster than ISC in $HzTFEX_2$ ($k_{RISC} = 4.2 \times 10^7\ s^{-1}$ versus $k_{ISC} = 2.3 \times 10^7\ s^{-1}$), whereas RISC is slower than ISC in $HzPipX_2$ ($k_{RISC} = 2.2 \times 10^7\ s^{-1}$ versus $k_{ISC} = 8.9 \times 10^7\ s^{-1}$) (Fig. 3e,f). These parameters simulate that the population of T_1 is lower than that of S_1 in $HzTFEX_2$ under the steady-state condition, indicating that S_1 lies energetically below T_1 (Extended Data Fig. 2). Furthermore, the temperature dependence of k_{ISC} and k_{RISC} follows the Arrhenius equation, $k = A\exp(-E_a/k_BT)$, in which k is the rate constant, A is the pre-exponential factor, E_a is the activation energy, k_B is the Boltzmann constant and T is the absolute temperature (Extended Data Fig. 3). The best-fit parameters of the Arrhenius equation yield the activation energies of ISC and RISC ($E_{a,ISC}$ and $E_{a,RISC}$) (Extended Data Table 1). Subtracting $E_{a,ISC}$ from $E_{a,RISC}$, we determined ΔE_{ST} of $HzTFEX_2$ to be -11 ± 2 meV, which is in marked contrast to positive ΔE_{ST} ever observed in numerous molecules, as well as in $HzPipX_2$ ($\Delta E_{ST} = 52 \pm 1$ meV). We note that the change in $k_r + k_{nr}$ at varying temperatures is negligible compared with those in k_{ISC} and k_{RISC} (Supplementary Fig. 4) and thus the decreasing trend of τ_{DF} of $HzTFEX_2$ is more reasonably attributed to the inverted S_1 and T_1. The negative ΔE_{ST} of $HzTFEX_2$ is retained in a solid-state host matrix (see Extended Data Fig. 4 and the Supplementary Information for details).

Having experimentally determined negative ΔE_{ST}, we conclude that $HzTFEX_2$ exhibits DFIST. Further synthetic efforts replacing the xylyl groups in $HzTFEX_2$ with either phenyl or tolyl groups led to $HzTFEP_2$ and $HzTFET_2$, which similarly show DFIST with measured ΔE_{ST} of -14 ± 3 meV and -13 ± 3 meV, respectively (see Extended Data Table 1 and Supplementary Fig. 5 for details), indicating the potential of heptazines for further developing efficient DFIST materials. In common with the three materials, ISC from S_1 to T_1 competes with the inherently slow radiative decay of heptazines, followed by faster RISC, leading to a significant S_1 population relative to T_1 and sub-microsecond DFIST. Thus, we propose to refer to the present type of emissions as 'H (heptazine)-type delayed fluorescence' by analogy with 'E (eosin)-type delayed fluorescence' referred to as TADF[42] and 'P (pyren)-type delayed fluorescence' involving triplet–triplet annihilation[43].

Finally, we evaluated the electroluminescence (EL) properties of $HzTFEX_2$ in OLEDs fabricated by thermal evaporation. The details of the fabrication procedures and the device structures are given in the Supplementary Information. Figure 4a,b shows the EL spectra, current density–voltage–luminance characteristics and external quantum efficiency–luminance characteristics of the OLED. Intense blue EL originating from $HzTFEX_2$ was observed with spectral peak wavelengths (λ_{EL}) at 450 nm and 479 nm and Commission internationale de l'éclairage (CIE) coordinates of (0.17, 0.24). The maximum external quantum efficiency reached 17%, corresponding to the internal quantum efficiency of 80% for a bottom-emission OLED with a typical light-outcoupling efficiency of 20%[44]. We note that the viewing-angle dependence of the luminance followed the Lambertian distribution (Fig. 4b inset), ensuring accurate estimation of the external quantum efficiency from the forward emission. Remarkably, $HzTFEX_2$ exhibited fast transient EL decay, reflecting the sub-microsecond H-type delayed fluorescence (Fig. 4c). In comparison, much slower transient EL decays were observed for E-type delayed fluorescence of 2,4,5,6-tetra(carbazol-9-yl)isophthalonitrile (4CzIPN)[6] and P-type delayed fluorescence of 2-methyl-9,10-bis(naphthalen-2-yl) anthracene (MADN)[45], although the EL of MADN initially decayed faster by the prompt fluorescence solely from S_1 (ref. [46]). It is thus evident that the fast triplet harvesting of $HzTFEX_2$ with negative ΔE_{ST} can be retained even in actual OLEDs. Although the efficiency roll-off is still marked in this preliminary device concerning the large hole injection barrier caused by the high ionization potential of $HzTFEX_2$ (6.3 eV), we anticipate that further optimization of molecular design will address this issue and allow a conclusive exploration of the effects of negative ΔE_{ST} on efficiency roll-off and device stability.

In conclusion, we have demonstrated fluorescent heptazine molecules that possess negative ΔE_{ST}. We observed their blue delayed fluorescence in both PL and EL with anomalous features: (1) the very short decay time constants ($\tau_{DF} \approx 0.2$ μs), (2) the decreasing trend of τ_{DF} with decreasing temperature and (3) the rate inversion of RISC and ISC ($k_{RISC} > k_{ISC}$). These features indeed arise from negative ΔE_{ST} and led to the terminology 'delayed fluorescence from inverted singlet and triplet

excited states (DFIST)' or 'H (heptazine)-type delayed fluorescence'. We predict that further development of DFIST materials will offer stable and efficient OLEDs based on the fast triplet-to-singlet downconversion, with great implications for displays, lighting and lasers.

Online content

Any methods, additional references, Nature Research reporting summaries, source data, extended data, supplementary information, acknowledgements, peer review information; details of author contributions and competing interests; and statements of data and code availability are available at https://doi.org/10.1038/s41586-022-05132-y.

1. Hund, F. Zur Deutung verwickelter Spektren, insbesondere der Elemente Scandium bis Nickel. *Z. Phys.* **33**, 345–371 (1925).
2. Baldo, M. A. et al. Highly efficient phosphorescent emission from organic electroluminescent devices. *Nature* **395**, 151–154 (1998).
3. Baldo, M. A., Lamansky, S., Burrows, P., Thompson, M. E. & Forrest, S. R. Very high-efficiency green organic light-emitting devices based on electrophosphorescence. *Appl. Phys. Lett.* **75**, 4–6 (1999).
4. Reineke, S. et al. White organic light-emitting diodes with fluorescent tube efficiency. *Nature* **459**, 234–238 (2009).
5. Endo, A. et al. Efficient up-conversion of triplet excitons into a singlet state and its application for organic light emitting diodes. *Appl. Phys. Lett.* **98**, 083302 (2011).
6. Uoyama, H., Goushi, K., Shizu, K., Nomura, H. & Adachi, C. Highly efficient organic light-emitting diodes from delayed fluorescence. *Nature* **492**, 234–238 (2012).
7. Liu, Y., Li, C., Ren, Z., Yan, S. & Bryce, M. R. All-organic thermally activated delayed fluorescence materials for organic light-emitting diodes. *Nat. Rev. Mater.* **3**, 18020 (2018).
8. Baldo, M. A., Adachi, C. & Forrest, S. R. Transient analysis of organic electrophosphorescence. II. Transient analysis of triplet-triplet annihilation. *Phys. Rev. B* **62**, 10967 (2000).
9. Murawski, C., Leo, K. & Gather, M. C. Efficiency roll-off in organic light-emitting diodes. *Adv. Mater.* **25**, 6801–6827 (2013).
10. Schmidbauer, S., Hohenleutner, A. & König, B. Chemical degradation in organic light-emitting devices: mechanisms and implications for the design of new materials. *Adv. Mater.* **25**, 2114–2129 (2013).
11. Slater, J. C. The theory of complex spectra. *Phys. Rev.* **34**, 1293 (1929).
12. Ziegler, T., Rauk, A. & Baerends, E. J. On the calculation of multiplet energies by the Hartree–Fock–Slater method. *Theor. Chem. Acc.* **43**, 261–271 (1977).
13. Leupin, W. & Wirz, J. Low-lying electronically excited states of cycl[3.3.3]azine, a bridged 12π-perimeter. *J. Am. Chem. Soc.* **102**, 6068–6075 (1980).
14. Leupin, W., Magde, D., Persy, G. & Wirz, J. 1,4,7-Triazacycl[3.3.3]azine: basicity, photoelectron spectrum, photophysical properties. *J. Am. Chem. Soc.* **108**, 17–22 (1986).
15. Ehrmaier, J. et al. Singlet–triplet inversion in heptazine and in polymeric carbon nitrides. *J. Phys. Chem. A* **123**, 8099–8108 (2019).
16. de Silva, P. Inverted singlet–triplet gaps and their relevance to thermally activated delayed fluorescence. *J. Phys. Chem. Lett.* **10**, 5674–5679 (2019).
17. Sanz-Rodrigo, J., Ricci, G., Olivier, Y. & Sancho-Garcia, J.-C. Negative singlet–triplet excitation energy gap in triangle-shaped molecular emitters for efficient triplet harvesting. *J. Phys. Chem. A* **125**, 513–522 (2021).
18. Ricci, G., San-Fabián, E., Olivier, Y. & Sancho-García, J.-C. Singlet-triplet excited-state inversion in heptazine and related molecules: assessment of TD-DFT and ab initio methods. *ChemPhysChem* **22**, 553–560 (2021).
19. Pollice, R., Friederich, P., Lavigne, C., dos Passos Gomes, G. & Aspuru-Guzik, A. Organic molecules with inverted gaps between first excited singlet and triplet states and appreciable fluorescence rates. *Matter* **4**, 1654–1682 (2021).
20. Sobolewski, A. L. & Domcke, W. Are heptazine-based organic light-emitting diode chromophores thermally activated delayed fluorescence or inverted singlet–triplet systems? *J. Phys. Chem. Lett.* **12**, 6852–6860 (2021).
21. Audebert, P., Kroke, E., Posern, C. & Lee, S.-H. State of the art in the preparation and properties of molecular monomeric *s*-heptazines: syntheses, characteristics, and functional applications. *Chem. Rev.* **121**, 2515–2544 (2021).
22. Hatakeyama, T. et al. Ultrapure blue thermally activated delayed fluorescence molecules: efficient HOMO–LUMO separation by the multiple resonance effect. *Adv. Mater.* **28**, 2777–2781 (2016).
23. Pershin, A. et al. Highly emissive excitons with reduced exchange energy in thermally activated delayed fluorescent molecules. *Nat. Commun.* **10**, 597 (2019).
24. Galmiche, L., Allain, C., Le, T., Guillot, R. & Audebert, P. Renewing accessible heptazine chemistry: 2,5,8-tris(3,5-diethyl-pyrazolyl)-heptazine, a new highly soluble heptazine derivative with exchangeable groups, and examples of newly derived heptazines and their physical chemistry. *Chem. Sci.* **10**, 5513–5518 (2019).
25. Le, T., Galmiche, L., Masson, G., Allain, C. & Audebert, P. A straightforward synthesis of a new family of molecules: 2,5,8-trialkoxyheptazines. Application to photoredox catalyzed transformations. *Chem. Commun.* **56**, 10742–10745 (2020).
26. Li, J. et al. Highly efficient organic light-emitting diode based on a hidden thermally activated delayed fluorescence channel in a heptazine derivative. *Adv. Mater.* **25**, 3319–3323 (2013).
27. Li, J., Zhang, Q., Nomura, H., Miyazaki, H. & Adachi, C. Thermally activated delayed fluorescence from $^3n\pi^*$ to $^1n\pi^*$ up-conversion and its application to organic light-emitting diodes. *Appl. Phys. Lett.* **105**, 013301 (2014).
28. Elliott, P., Goldson, S., Canahui, C. & Maitra, N. T. Perspectives on double-excitations in TDDFT. *Chem. Phys.* **391**, 110–119 (2011).
29. Stanton, J. F. & Bartlett, R. J. The equation of motion coupled-cluster method. A systematic biorthogonal approach to molecular excitation energies, transition probabilities, and excited state properties. *J. Chem. Phys.* **98**, 7029–7039 (1993).
30. Di, D. et al. High-performance light-emitting diodes based on carbene-metal-amides. *Science* **356**, 159–163 (2017).
31. Zeng, W. et al. Achieving nearly 30% external quantum efficiency for orange–red organic light emitting diodes by employing thermally activated delayed fluorescence emitters composed of 1,8-naphthalimide-acridine hybrids. *Adv. Mater.* **30**, 1704961 (2018).
32. Wu, T.-L. et al. Diboron compound-based organic light-emitting diodes with high efficiency and reduced efficiency roll-off. *Nat. Photonics* **12**, 235–240 (2018).
33. Dos Santos, P. L. et al. Triazatruxene: a rigid central donor unit for a D–A_3 thermally activated delayed fluorescence material exhibiting sub-microsecond reverse intersystem crossing and unity quantum yield via multiple singlet–triplet state pairs. *Adv. Sci.* **5**, 1700989 (2018).
34. Kondo, Y. et al. Narrowband deep-blue organic light-emitting diode featuring an organoboron-based emitter. *Nat. Photonics* **13**, 678–682 (2019).
35. Hamze, R. et al. Eliminating nonradiative decay in Cu(I) emitters: >99% quantum efficiency and microsecond lifetime. *Science* **363**, 601–606 (2019).
36. Kim, J. U. et al. Nanosecond-time-scale delayed fluorescence molecule for deep-blue OLEDs with small efficiency rolloff. *Nat. Commun.* **11**, 1765 (2020).
37. Cui, L.-S. et al. Fast spin-flip enables efficient and stable organic electroluminescence from charge-transfer states. *Nat. Photonics* **14**, 636–642 (2020).
38. Wada, Y., Nakagawa, H., Matsumoto, S., Wakisaka, Y. & Kaji, H. Organic light emitters exhibiting very fast reverse intersystem crossing. *Nat. Photonics* **14**, 643–649 (2020).
39. Martin, R. L. Natural transition orbitals. *J. Chem. Phys.* **118**, 4775–4777 (2003).
40. Schirmer, J. Beyond the random-phase approximation: a new approximation scheme for the polarization propagator. *Phys. Rev. A* **26**, 2395 (1982).
41. Andersson, K., Malmqvist, P. Å. & Roos, B. O. Second-order perturbation theory with a complete active space self-consistent field reference function. *J. Chem. Phys.* **96**, 1218–1226 (1992).
42. Parker, C. & Hatchard, C. Triplet-singlet emission in fluid solutions. Phosphorescence of eosin. *Trans. Faraday Soc.* **57**, 1894–1904 (1961).
43. Parker, C. Sensitized *P*-type delayed fluorescence. *Proc. R. Soc. Lond. A Math. Phys. Sci.* **276**, 125–135 (1963).
44. Nowy, S., Krummacher, B. C., Frischeisen, J., Reinke, N. A. & Brütting, W. Light extraction and optical loss mechanisms in organic light-emitting diodes: influence of the emitter quantum efficiency. *J. Appl. Phys.* **104**, 123109 (2008).
45. Lee, M.-T., Chen, H.-H., Liao, C.-H., Tsai, C.-H. & Chen, C. H. Stable styrylamine-doped blue organic electroluminescent device based on 2-methyl-9,10-*di*(2-naphthyl)anthracene. *Appl. Phys. Lett.* **85**, 3301–3303 (2004).
46. Pu, Y.-J. et al. Absence of delayed fluorescence and triplet–triplet annihilation in organic light emitting diodes with spatially orthogonal bianthracenes. *J. Mater. Chem. C* **7**, 2541–2547 (2019).

Publisher's note Springer Nature remains neutral with regard to jurisdictional claims in published maps and institutional affiliations.

Open Access This article is licensed under a Creative Commons Attribution 4.0 International License, which permits use, sharing, adaptation, distribution and reproduction in any medium or format, as long as you give appropriate credit to the original author(s) and the source, provide a link to the Creative Commons license, and indicate if changes were made. The images or other third party material in this article are included in the article's Creative Commons license, unless indicated otherwise in a credit line to the material. If material is not included in the article's Creative Commons license and your intended use is not permitted by statutory regulation or exceeds the permitted use, you will need to obtain permission directly from the copyright holder. To view a copy of this license, visit http://creativecommons.org/licenses/by/4.0/.

© The Author(s) 2022

Methods

Quantum-chemical calculations

For the 34,596 heptazine molecules, the T_1 geometries were optimized using spin-unrestricted DFT with the LC-BLYP functional and the 6-31G basis set. Vibrational frequency analysis for $HzTFEX_2$, $HzPipX_2$, $HzTFEP_2$ and $HzTFET_2$ gave no imaginary frequencies at the same level of theory. The vertical excitation energies of S_1 and T_1 were calculated using liner-response TDDFT with the LC-BLYP functional and the 6-31G(d) basis set within the Tamm–Dancoff approximation. The range-separation parameter of the LC-BLYP functional was non-empirically optimized to 0.18 $bohr^{-1}$ to minimize the difference between the energy of the HOMO and the ionization potential of the neutral system and the difference between the energy of the HOMO of the radical anion system and the electron affinity of the neutral system[47] of 2,5,8-triphenylheptazine. The T_1 geometries of $HzTFEX_2$ and $HzPipX_2$ were also optimized using spin-unrestricted second-order Møller–Plesset perturbation theory (MP2) with the correlation consistent cc-pVDZ basis set. At the MP2 geometries of $HzTFEX_2$ and $HzPipX_2$, the vertical excitation energies of S_1 and T_1 were calculated using EOM-CCSD[29], ADC(2)[40] and CASPT2[41] with the cc-pVDZ basis set. The CASPT2 calculations were performed with the fully internally contracted scheme over the state-averaged complete active space self-consistent field (CASSCF) wavefunctions with the active space of 12 electrons and 12 orbitals using the resolution of identity approximation with the auxiliary fitting basis set. The DFT, TDDFT, MP2 and EOM-CCSD calculations were performed using the Gaussian 16 Rev C.01 program. The ADC(2) calculations were performed using the Q-Chem 5.3.0 program. The CASSCF and CASPT2 calculations were performed using the Orca 4.2.1 program.

Materials and synthesis

Commercially available reagents and solvents were used without further purification unless otherwise noted. 4CzIPN and MADN were purchased from Luminescence Technology Corporation and e-Ray Optoelectronics Technology, respectively. The synthetic procedures and characterization data of the heptazine molecules are detailed in the Supplementary Information.

Photophysical measurements

Steady-state ultraviolet–visible absorption spectra were recorded on a Shimadzu UV-3600i Plus spectrophotometer. Steady-state PL spectra were acquired on a HORIBA FL3 spectrofluorometer with 370-nm photoexcitation from a Xe arc lamp. The absolute PL quantum yields were determined using a Hamamatsu Photonics C9920 integrated sphere system with 370-nm excitation from a Xe arc lamp. Transient absorption decay measurements were performed by a randomly interleaved plus train method[48] on a UNISOKU picoTAS system with a 355-nm Q-switched laser pump source (pulse width <350 ps) and a supercontinuum white probe source (pulse width <100 ps). Transient PL decay measurements were performed by time-correlated single-photon counting on a HORIBA FL3 spectrofluorometer with a 370-nm LED pump source (pulse width <1.2 ns) and a UNISOKU CoolSpek cryostat using liquid nitrogen as the coolant. Ionization potentials were determined using a RIKEN KEIKI AC-3 ultraviolet photoelectron yield spectrometer.

Analysis of transient PL decay kinetics

The time constants of prompt and delayed fluorescence (τ_{PF} and τ_{DF}) were determined by biexponential decay fitting and deconvolution with the instrument response function. It is common when determining the rate constants of the transitions involved in TADF to assume $k_{ISC} >> k_{RISC}$ such that the contribution of RISC to the prompt fluorescence is negligible[49]. However, this assumption does not hold true for DFIST materials with $k_{RISC} > k_{ISC}$. Thus, $k_r + k_{nr}$, k_{ISC} and k_{RISC} were determined without assuming $k_{ISC} >> k_{RISC}$ by fitting the S_1 population in equation (1) to the transient PL decay data using the scipy.integrate.odeint and scipy.optimize.curve_fit functions in Python 3.7[50]. k_r and k_{nr} were determined from $\Phi_{PL} = k_r/(k_r + k_{nr})$ assuming negligible non-radiative decay of T_1 to S_0. Activation energies of ISC and RISC ($E_{a,ISC}$ and $E_{a,RISC}$) were determined by fitting the Arrhenius equation to the temperature dependence of k_{ISC} and k_{RISC}, respectively. ΔE_{ST} was determined by subtracting $E_{a,ISC}$ from $E_{a,RISC}$.

OLED fabrication and evaluation

The fabrication procedures of OLEDs are detailed in the Supplementary Information. EL spectra were recorded using a Hamamatsu Photonics PMA-12 photonic multichannel analyser. Current density–voltage–luminance characteristics were measured using a Konica Minolta CS-200 luminance meter and a Keithley 2400 source meter. The viewing-angle dependence of luminance was measured using a home-build spectro-goniometer with a Konica Minolta CS-2000 spectroradiometer. Transient EL decays measurements were performed using a home-build set-up with a Hamamatsu Photonics H7826 silicon photomultiplier tube (time response = 1.5 ns) and an Agilent 33220A function generator for pulse OLED operation (square-wave voltages = 8, −4 V and frequency = 2 kHz).

Reporting summary

Further information on research design is available in the Nature Research Reporting Summary linked to this article.

Data availability

The data underlying this article are available at https://doi.org/10.6084/m9.figshare.20058977.

47. Baer, R., Livshits, E. & Salzner, U. Tuned range-separated hybrids in density functional theory. *Annu. Rev. Phys. Chem.* **61**, 85–109 (2010).
48. Nakagawa, T., Okamoto, K., Hanada, H. & Katoh, R. Probing with randomly interleaved pulse train bridges the gap between ultrafast pump-probe and nanosecond flash photolysis. *Opt. Lett.* **41**, 1498–1501 (2016).
49. Goushi, K., Yoshida, K., Sato, K. & Adachi, C. Organic light-emitting diodes employing efficient reverse intersystem crossing for triplet-to-singlet state conversion. *Nat. Photonics* **6**, 253–258 (2012).
50. Haase, N. et al. Kinetic modeling of transient photoluminescence from thermally activated delayed fluorescence. *J. Phys. Chem. C* **122**, 29173–29179 (2018).

Acknowledgements This work was supported in part by an Industrial Technology Research Grant for Young Researchers from the New Energy and Industrial Technology Development Organization (NEDO) (grant no. 09151455 to Y.-J.P.), JST PRESTO (grant nos. 13417316 to Y.-J.P. and JPMJPR17N1 to N.A.) and JSPS KAKENHI (grant nos. 24685029, 17H03103, 20H02554 to Y.-J.P. and 20K15252, 21H05413, 22H02051 to N.A.). The authors thank M. Kim at RIKEN CEMS, T. Chiba, and M. Hirasawa at Yamagata University for their support with the OLED fabrication and evaluation. The computations were partially performed using the HOKUSAI Big Waterfall system at RIKEN.

Author contributions N.A. and D.M. conceived the project. N.A., Y.H. and S.M. conceived the procedures of the computational calculations. N.A., Y.-J.P., Y.H., K.N. and S.M. performed the computational calculations. N.A., H.I. and Y.-J.P. performed the photophysical measurements. N.A., Y.K. and Y.-J.P. fabricated and evaluated the OLEDs. B.D., R.I., H.I. and A.N. performed synthetic experiments and assisted the characterization of the synthesized compounds and analysis of data. N.A., Y.-J.P., F.A. and D.M. designed the experiments and analysed the data. N.A., Y.-J.P. and D.M. wrote the manuscript.

Competing interests The authors declare no competing interests.

Additional information
Supplementary information The online version contains supplementary material available at https://doi.org/10.1038/s41586-022-05132-y.

Correspondence and requests for materials should be addressed to Naoya Aizawa, Yong-Jin Pu or Daigo Miyajima.

Peer review information *Nature* thanks Pierre Audebert and the other, anonymous, reviewer(s) for their contribution to the peer review of this work. Peer reviewer reports are available.

Reprints and permissions information is available at http://www.nature.com/reprints.

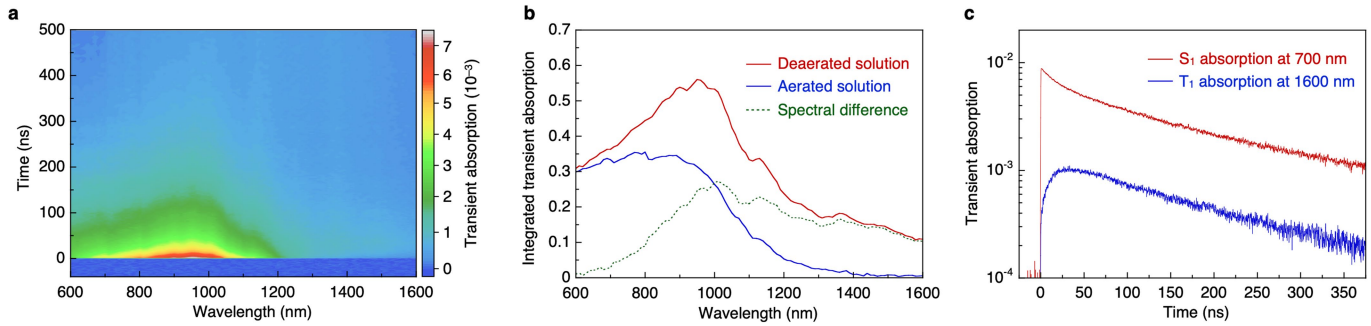

Extended Data Fig. 1 | Transient absorption data of $HzTFEX_2$. a, Transient absorption of $HzTFEX_2$ as a function of wavelength and time in a deaerated toluene solution. **b**, Integrated transient absorption spectra of $HzTFEX_2$ over 0–500 ns in deaerated and aerated toluene solutions; the dashed green dashed line represents their spectral difference and mainly corresponds to the transient absorption of T_1. **c**, Transient absorption decays of S_1 and T_1 monitored at 700 nm and 1,600 nm, respectively.

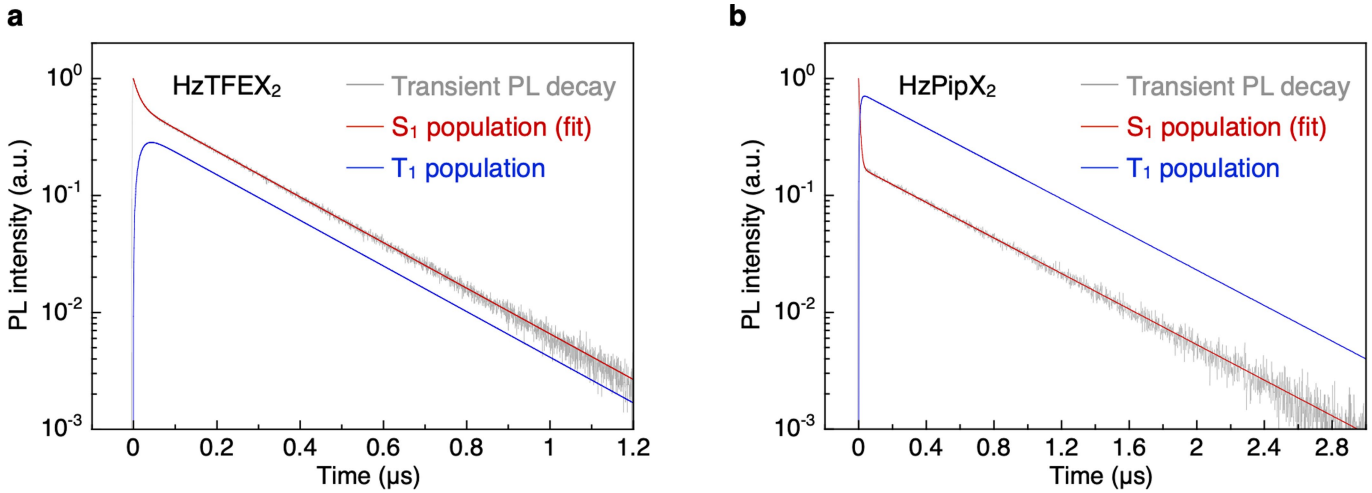

Extended Data Fig. 2 | Analysis of the transient PL decays of $HzTFEX_2$ and $HzPipX_2$. a,**b**, Fit (solid red line) of the S_1 population in equation (1) to the transient PL decay of $HzTFEX_2$ (**a**) and $HzPipX_2$ (**b**) in deaerated toluene solutions at 300 K. The solid blue line represents the T_1 population simulated by the best-fit parameters $k_r + k_{nr}$, k_{ISC} and k_{RISC} in equation (1).

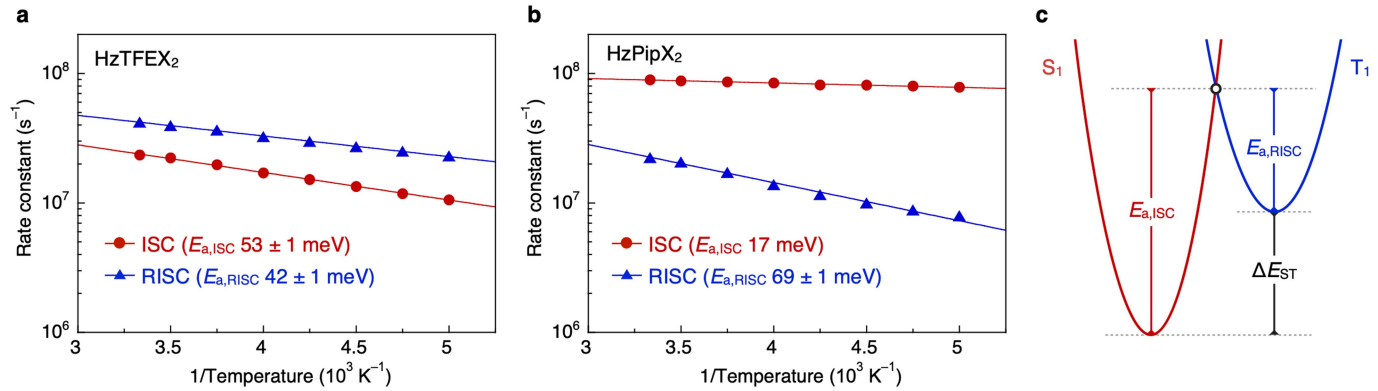

Extended Data Fig. 3 | k_{ISC} and k_{RISC} of $HzTFEX_2$ and $HzPipX_2$. a,**b**, Temperature dependence of k_{ISC} and k_{RISC} of $HzTFEX_2$ (**a**) and $HzPipX_2$ (**b**) in deaerated toluene. The solid lines in **a** and **b** represent the fits of the plots to the Arrhenius equation. The error bars of the plots in **a** and **b** are smaller than the plot size. **c**, Schematic diagram of the potential energy surfaces of S_1 and T_1 and the activation energies of ISC and RISC.

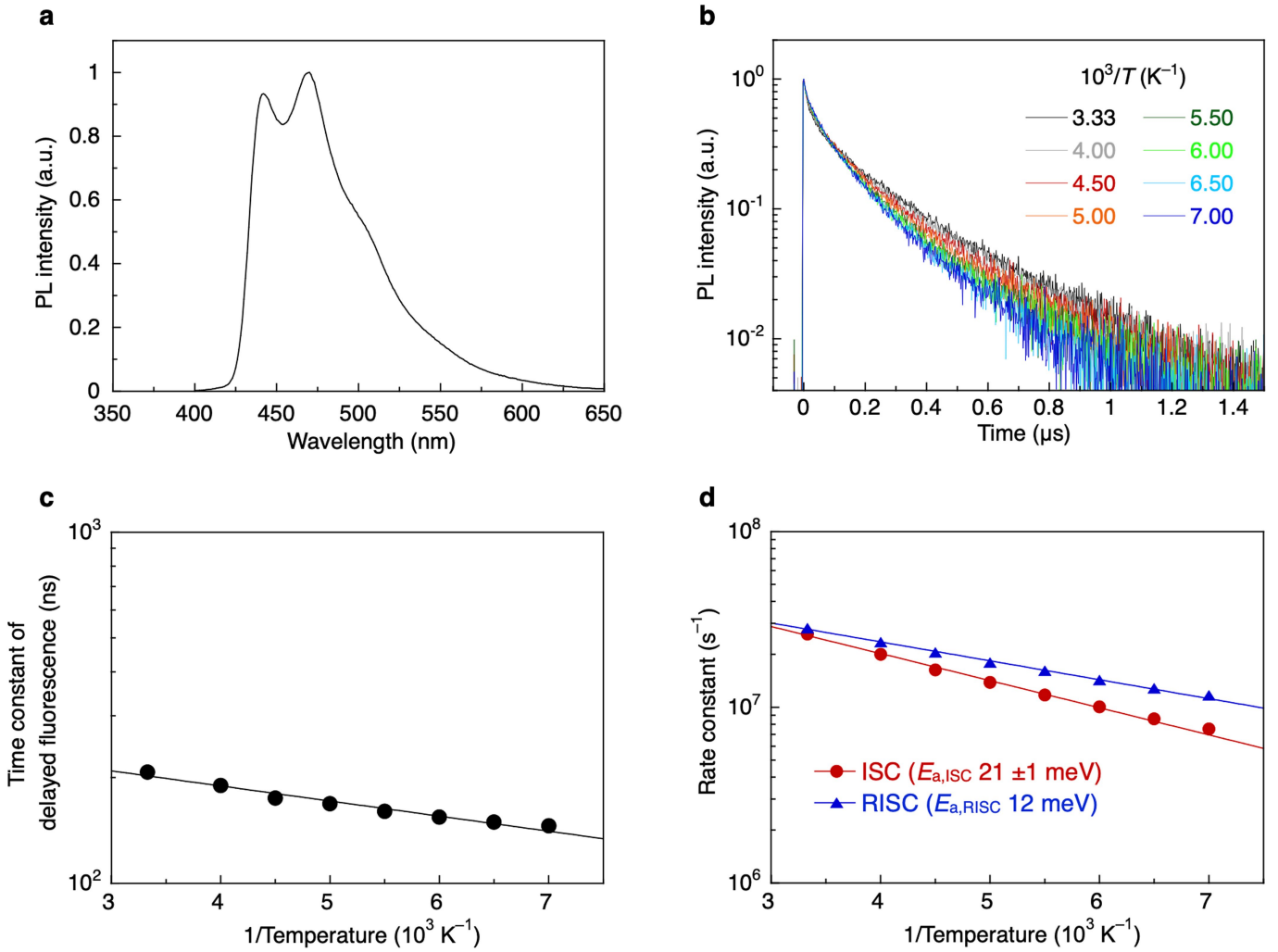

Extended Data Fig. 4 | Photophysical properties of HzTFEX$_2$ in a solid-state host matrix. a, Steady-state PL spectra of a thin film of bis(diphenylphosphoryl) dibenzo[*b*,*d*]furan (PPF):1 wt% HzTFEX$_2$. **b**, Transient PL decays of PPF:1 wt% HzTFEX$_2$ at varying temperatures under a N_2 atmosphere. **c**, Temperature dependence of τ_{DF} of PPF:1 wt% HzTFEX$_2$. **d**, Temperature dependence of k_{ISC} and k_{RISC} of PPF:1 wt% HzTFEX$_2$. The solid lines in **d** represent the fits of the plots to the Arrhenius equation.

Extended Data Table 1 | Photophysical properties of $HzTFEX_2$ and $HzPipX_2$ in deaerated toluene solutions

Emitter	λ_{PL} (nm)[a]	Φ_{PL} (%)[b]	τ_{PF} (ns)[c]	τ_{DF} (ns)[d]	k_r (s^{-1})[e]	k_{nr} (s^{-1})[f]	k_{ISC} (s^{-1})[g]	k_{RISC} (s^{-1})[h]	$E_{a,ISC}$ (meV)[i]	$E_{a,RISC}$ (meV)[j]	ΔE_{ST} (meV)[k]
$HzTFEX_2$	449, 476	74	14	217	5.4×10^6	1.9×10^6	2.3×10^7	4.2×10^7	53 ± 1	42 ± 1	–11 ± 2
$HzPipX_2$	442, 467	67	7.9	565	6.3×10^6	3.1×10^6	8.9×10^7	2.2×10^7	17	69 ± 1	52 ± 1
$HzTFEP_2$	454, 483	44	35	288	3.1×10^6	4.0×10^6	1.4×10^7	1.8×10^7	31 ± 2	17 ± 1	–14 ± 3
$HzTFET_2$	451, 479	42	23	246	2.9×10^6	4.0×10^6	1.6×10^7	2.7×10^7	44 ± 2	31 ± 1	–13 ± 3

[a]Photoluminescence (PL) peak wavelength. [b]PL quantum yield. [c]Time constant of prompt fluorescence. [d]Time constant of delayed fluorescence. [e]Rate constant of radiative decay of the lowest-energy excited state (S_1) to the ground state (S_0). [f]Rate constant of non-radiative decay of S_1 to S_0. [g]Rate constant of intersystem crossing (ISC) of S_1 to the lowest-energy triplet excited state (T_1). [h]Rate constant of reverse intersystem crossing (RISC) of T_1 to S_1. [i]Activation energy of ISC. [j]Activation energy of RISC. [k]Energy gap between S_1 and T_1.

nature portfolio

Corresponding author(s): Naoya Aizawa

Last updated by author(s): Jun 14, 2022

Reporting Summary

Nature Portfolio wishes to improve the reproducibility of the work that we publish. This form provides structure for consistency and transparency in reporting. For further information on Nature Portfolio policies, see our Editorial Policies and the Editorial Policy Checklist.

Statistics

For all statistical analyses, confirm that the following items are present in the figure legend, table legend, main text, or Methods section.

n/a	Confirmed
☐	☒ The exact sample size (*n*) for each experimental group/condition, given as a discrete number and unit of measurement
☐	☒ A statement on whether measurements were taken from distinct samples or whether the same sample was measured repeatedly
☐	☒ The statistical test(s) used AND whether they are one- or two-sided *Only common tests should be described solely by name; describe more complex techniques in the Methods section.*
☐	☒ A description of all covariates tested
☐	☒ A description of any assumptions or corrections, such as tests of normality and adjustment for multiple comparisons
☐	☒ A full description of the statistical parameters including central tendency (e.g. means) or other basic estimates (e.g. regression coefficient) AND variation (e.g. standard deviation) or associated estimates of uncertainty (e.g. confidence intervals)
☐	☒ For null hypothesis testing, the test statistic (e.g. *F*, *t*, *r*) with confidence intervals, effect sizes, degrees of freedom and *P* value noted *Give P values as exact values whenever suitable.*
☐	☒ For Bayesian analysis, information on the choice of priors and Markov chain Monte Carlo settings
☐	☒ For hierarchical and complex designs, identification of the appropriate level for tests and full reporting of outcomes
☐	☒ Estimates of effect sizes (e.g. Cohen's *d*, Pearson's *r*), indicating how they were calculated

Our web collection on statistics for biologists contains articles on many of the points above.

Software and code

Policy information about availability of computer code

Data collection	Quantum chemical calculations were performed using Gaussian 16 RevC.01, Q-Chem 5.3.0, Orca 4.2.1, and MOLPRO 2019.2.
Data analysis	The numerical fit of the S1 population in Eq. (1) to the transient PL decay data was performed using the scipy.integrate.odeint and scipy.optimize.curve_fit functions in Python 3.7.

For manuscripts utilizing custom algorithms or software that are central to the research but not yet described in published literature, software must be made available to editors and reviewers. We strongly encourage code deposition in a community repository (e.g. GitHub). See the Nature Portfolio guidelines for submitting code & software for further information.

Data

Policy information about availability of data

All manuscripts must include a data availability statement. This statement should provide the following information, where applicable:

- Accession codes, unique identifiers, or web links for publicly available datasets
- A description of any restrictions on data availability
- For clinical datasets or third party data, please ensure that the statement adheres to our policy

The data underlying this article are available at https://doi.org/10.6084/m9.figshare.20058977. (The DOI will become active when the paper is published.)

Human research participants

Policy information about studies involving human research participants and Sex and Gender in Research.

Reporting on sex and gender	*Use the terms sex (biological attribute) and gender (shaped by social and cultural circumstances) carefully in order to avoid confusing both terms. Indicate if findings apply to only one sex or gender; describe whether sex and gender were considered in study design whether sex and/or gender was determined based on self-reporting or assigned and methods used. Provide in the source data disaggregated sex and gender data where this information has been collected, and consent has been obtained for sharing of individual-level data; provide overall numbers in this Reporting Summary. Please state if this information has not been collected. Report sex- and gender-based analyses where performed, justify reasons for lack of sex- and gender-based analysis.*
Population characteristics	*Describe the covariate-relevant population characteristics of the human research participants (e.g. age, genotypic information, past and current diagnosis and treatment categories). If you filled out the behavioural & social sciences study design questions and have nothing to add here, write "See above."*
Recruitment	*Describe how participants were recruited. Outline any potential self-selection bias or other biases that may be present and how these are likely to impact results.*
Ethics oversight	*Identify the organization(s) that approved the study protocol.*

Note that full information on the approval of the study protocol must also be provided in the manuscript.

Field-specific reporting

Please select the one below that is the best fit for your research. If you are not sure, read the appropriate sections before making your selection.

☐ Life sciences ☐ Behavioural & social sciences ☐ Ecological, evolutionary & environmental sciences

For a reference copy of the document with all sections, see nature.com/documents/nr-reporting-summary-flat.pdf

Life sciences study design

All studies must disclose on these points even when the disclosure is negative.

Sample size	*Describe how sample size was determined, detailing any statistical methods used to predetermine sample size OR if no sample-size calculation was performed, describe how sample sizes were chosen and provide a rationale for why these sample sizes are sufficient.*
Data exclusions	*Describe any data exclusions. If no data were excluded from the analyses, state so OR if data were excluded, describe the exclusions and the rationale behind them, indicating whether exclusion criteria were pre-established.*
Replication	*Describe the measures taken to verify the reproducibility of the experimental findings. If all attempts at replication were successful, confirm this OR if there are any findings that were not replicated or cannot be reproduced, note this and describe why.*
Randomization	*Describe how samples/organisms/participants were allocated into experimental groups. If allocation was not random, describe how covariates were controlled OR if this is not relevant to your study, explain why.*
Blinding	*Describe whether the investigators were blinded to group allocation during data collection and/or analysis. If blinding was not possible, describe why OR explain why blinding was not relevant to your study.*

Behavioural & social sciences study design

All studies must disclose on these points even when the disclosure is negative.

Study description	*Briefly describe the study type including whether data are quantitative, qualitative, or mixed-methods (e.g. qualitative cross-sectional, quantitative experimental, mixed-methods case study).*
Research sample	*State the research sample (e.g. Harvard university undergraduates, villagers in rural India) and provide relevant demographic information (e.g. age, sex) and indicate whether the sample is representative. Provide a rationale for the study sample chosen. For studies involving existing datasets, please describe the dataset and source.*
Sampling strategy	*Describe the sampling procedure (e.g. random, snowball, stratified, convenience). Describe the statistical methods that were used to predetermine sample size OR if no sample-size calculation was performed, describe how sample sizes were chosen and provide a rationale for why these sample sizes are sufficient. For qualitative data, please indicate whether data saturation was considered, and what criteria were used to decide that no further sampling was needed.*

Data collection	*Provide details about the data collection procedure, including the instruments or devices used to record the data (e.g. pen and paper, computer, eye tracker, video or audio equipment) whether anyone was present besides the participant(s) and the researcher, and whether the researcher was blind to experimental condition and/or the study hypothesis during data collection.*
Timing	*Indicate the start and stop dates of data collection. If there is a gap between collection periods, state the dates for each sample cohort.*
Data exclusions	*If no data were excluded from the analyses, state so OR if data were excluded, provide the exact number of exclusions and the rationale behind them, indicating whether exclusion criteria were pre-established.*
Non-participation	*State how many participants dropped out/declined participation and the reason(s) given OR provide response rate OR state that no participants dropped out/declined participation.*
Randomization	*If participants were not allocated into experimental groups, state so OR describe how participants were allocated to groups, and if allocation was not random, describe how covariates were controlled.*

Ecological, evolutionary & environmental sciences study design

All studies must disclose on these points even when the disclosure is negative.

Study description	*Briefly describe the study. For quantitative data include treatment factors and interactions, design structure (e.g. factorial, nested, hierarchical), nature and number of experimental units and replicates.*
Research sample	*Describe the research sample (e.g. a group of tagged Passer domesticus, all Stenocereus thurberi within Organ Pipe Cactus National Monument), and provide a rationale for the sample choice. When relevant, describe the organism taxa, source, sex, age range and any manipulations. State what population the sample is meant to represent when applicable. For studies involving existing datasets, describe the data and its source.*
Sampling strategy	*Note the sampling procedure. Describe the statistical methods that were used to predetermine sample size OR if no sample-size calculation was performed, describe how sample sizes were chosen and provide a rationale for why these sample sizes are sufficient.*
Data collection	*Describe the data collection procedure, including who recorded the data and how.*
Timing and spatial scale	*Indicate the start and stop dates of data collection, noting the frequency and periodicity of sampling and providing a rationale for these choices. If there is a gap between collection periods, state the dates for each sample cohort. Specify the spatial scale from which the data are taken*
Data exclusions	*If no data were excluded from the analyses, state so OR if data were excluded, describe the exclusions and the rationale behind them, indicating whether exclusion criteria were pre-established.*
Reproducibility	*Describe the measures taken to verify the reproducibility of experimental findings. For each experiment, note whether any attempts to repeat the experiment failed OR state that all attempts to repeat the experiment were successful.*
Randomization	*Describe how samples/organisms/participants were allocated into groups. If allocation was not random, describe how covariates were controlled. If this is not relevant to your study, explain why.*
Blinding	*Describe the extent of blinding used during data acquisition and analysis. If blinding was not possible, describe why OR explain why blinding was not relevant to your study.*

Did the study involve field work? ☐ Yes ☒ No

Reporting for specific materials, systems and methods

We require information from authors about some types of materials, experimental systems and methods used in many studies. Here, indicate whether each material, system or method listed is relevant to your study. If you are not sure if a list item applies to your research, read the appropriate section before selecting a response.

Materials & experimental systems

n/a	Involved in the study
☒	☐ Antibodies
☒	☐ Eukaryotic cell lines
☒	☐ Palaeontology and archaeology
☒	☐ Animals and other organisms
☒	☐ Clinical data
☒	☐ Dual use research of concern

Methods

n/a	Involved in the study
☒	☐ ChIP-seq
☒	☐ Flow cytometry
☒	☐ MRI-based neuroimaging